

Localization Limitations of ARCore, ARKit, and Hololens in Dynamic Large-scale Industry Environments

Tobias Feigl^{1,2}, Andreas Porada¹, Steve Steiner¹, Christoffer Löffler^{1,3}, Christopher Mutschler^{1,3} and Michael Philippsen²

¹Machine Learning and Information Fusion Group, Fraunhofer Institute for Integrated Circuits IIS, Nürnberg, Germany

²Programming Systems Group, Friedrich-Alexander University (FAU), Erlangen-Nürnberg, Germany

³Machine Learning and Data Analytics Lab, Friedrich-Alexander University (FAU), Erlangen-Nürnberg, Germany

Keywords: Augmented Reality (AR), Simultaneous Localization and Mapping (SLAM), Industry 4.0, Apple ARKit, Google ARCore, Microsoft Hololens.

Abstract: Augmented Reality (AR) systems are envisioned to soon be used as smart tools across many Industry 4.0 scenarios. The main promise is that such systems will make workers more productive when they can obtain additional situationally coordinated information both seamlessly and hands-free. This paper studies the applicability of today's popular AR systems (Apple ARKit, Google ARCore, and Microsoft Hololens) in such an industrial context (large area of $1,600m^2$, long walking distances of $60m$ between cubicles, and dynamic environments with volatile natural features). With an elaborate measurement campaign that employs a sub-millimeter accurate optical localization system, we show that for such a context, i.e., when a reliable and accurate tracking of a user matters, the Simultaneous Localization and Mapping (SLAM) techniques of these AR systems are a showstopper. Out of the box, these AR systems are far from useful even for normal motion behavior. They accumulate an average error of about $17m$ per $120m$, with a scaling error of up to $14.4cm/m$ that is quasi-directly proportional to the path length. By adding natural features, the tracking reliability can be improved, but not enough.

1 INTRODUCTION

The availability of Apple's ARKit, Google's ARCore, and Microsoft's Hololens, called AR_A (Dilek and Erol, 2018), AR_G (Voinea et al., 2018), and AR_M (Vassallo et al., 2017) below, with their built-in inside-out tracking technology that allows an accurate estimation of a user's pose, i.e., his/her head orientation and position, in small areas ($5m \times 5m$) has kindled the interest of industry in low-cost, self-localization-based AR technology (Klein and Murray, 2007; Linowes and Babilinski, 2017), to fully embed virtual content into the real environment (Feigl et al., 2018; Regenbrecht et al., 2017).

To avoid collisions between users and the environment that may be caused by misperceptions of the environment (Dilek and Erol, 2018), accurate and reliable pose estimates are needed. Thus, Visual-Inertial Simultaneous Localization and Mapping (VISLAM) has been invented (Liu et al., 2018; Taketomi et al., 2017; Terashima and Hasegawa, 2017; Kasyanov et al., 2017). It combines the camera's RGB (Li et al.,

2017) or RGB-D (Mur-Artal and Tardos, 2017; Kerl et al., 2013) signals with inertial sensor data from the headset (Kasyanov et al., 2017) to extract unique synthetic (Kato and Billinghurst, 1999; Marques et al., 2018) or natural (Neumann and You, 1999; Simon et al., 2000) features from the environment. With computationally intensive algorithms this works well on indoor and outdoor scenarios, at least on laborious datasets like KITTI (Geiger et al., 2013) and TUM (Schubert et al., 2018).

Unfortunately, current mobile AR systems have limited computational resources and thus only use a stripped down version of the latest, advanced VISLAM techniques (Liu et al., 2018; Taketomi et al., 2017; Terashima and Hasegawa, 2017). AR_A and AR_G (Linowes and Babilinski, 2017) seem to use VISLAM to register 3D poses and AR_M seems to use a combination of VISLAM and RGB-D (Mur-Artal and Tardos, 2017; Kerl et al., 2013; Vassallo et al., 2017).

The purpose of this study is to find out whether the stripped down SLAM technology built into these AR systems suffices for daily use in industry settings.

In an elaborate campaign we thus measure the accuracy and precision of the initialization, localization, and relocalization with a sub-millimeter accurate optical reference localization system. We study both the scaling errors and the reliability, i.e., the robustness with respect to fail-safety of the localization. And we investigate how the number of features influences the localization performance. We do all of this for three scenarios: self-motion in a *static*-environment, self-motion in a *dynamic*-environment, and *mixed* variants (both self- and object-motion).

Our evaluation shows that these AR systems do not yet work well enough for large-scale (industrial) environments. The main reasons are that the typical camera-based problems (such as poor lighting conditions, inadequate geometry, low structural complexity of the environment, and dynamics in the images, i.e., motion blur) cause a drift in the scaling of the environment map and a divergence of the real and virtual SLAM maps (Klein and Murray, 2007). The mismatch is even worse if self- and object-motion cannot be separated correctly (Li et al., 2018). The lack of reference points in the environment that otherwise may be used to reset scaling errors further limits their applicability in large-scale industry settings (Fraga-Lamas et al., 2018; Liu et al., 2018).

The paper is structured as follows. We discuss related work in Sec. 2. Sec. 3 describes the problem. We introduce our evaluation scheme in Sec. 4. Sec. 5 discusses evaluation results before Sec. 7 concludes.

2 RELATED WORK

In the following we discuss relevant publications that range from the challenges of current SLAM methods in AR (Dilek and Erol, 2018; Linowes and Babilinski, 2017; Vassallo et al., 2017; Li et al., 2017), over general technical challenges of commercial AR systems, to the applicability and usability of modern AR systems in industry settings (Fraga-Lamas et al., 2018; Palmarini et al., 2017; Klein and Murray, 2007). Here, some researchers also address specific industry applications and discuss the needs and difficulties of AR systems (Marchand et al., 2016; Yan and Hu, 2017). Finally, we discuss publicly available datasets that are commonly used to evaluate SLAM methods.

SLAM in AR Systems. Motion tracking has long been a research focus in the areas of computer vision and robotics. 3D point registration methods such as SLAM are the key for achieving immersive AR effects and for accurately registering and locating a person's pose in real time in an unknown environment.

Early AR solutions such as ARToolkit (Linowes and Babilinski, 2017) and Vuforia (Marchand et al., 2016) use synthetic registration markers which restrict AR objects to specific locations. Today, most camera tracking methods are based on natural features. Visual SLAM (VSLAM) has made remarkable progress over the last decade (Taketomi et al., 2017; Marchand et al., 2016; Kasyanov et al., 2017; Li et al., 2018; Mur-Artal and Tardos, 2017; Terashima and Hasegawa, 2017), enabling a real-time indoor and outdoor use, but still suffers heavily from scaling errors of the real and estimated maps.

When there is enough computational performance available, Visual Inertial SLAM (VISLAM) can combine VSLAM with Inertial Measurement Unit (IMU) sensors (accelerometer, gyroscope, and magnetometer) to partly resolve the scale ambiguity, to provide motion cues without visual features (Liu et al., 2018; Kasyanov et al., 2017), to process more features, and to make the tracking more robust (Taketomi et al., 2017; Kerl et al., 2013). We claim that AR_A , AR_G , and AR_M have limited computational capacity, need to save battery, and hence cannot process enough features to achieve a high tracking accuracy.

Technical Challenges of Commercial AR Systems. While vendors keep the exact implementation of SLAM in their systems secret and hence prevent application-based fine-tuning, there are several other technical constraints that limit the tracking performance of these products: The algorithms in AR_A (Dilek and Erol, 2018) are not only completely closed source, but also limited to Apple hardware and iOS. AR_G (Linowes and Babilinski, 2017) suffers from performance bottlenecks due to hardware limitations on Android devices. AR_M (Vassallo et al., 2017) only exposes its SLAM through a narrow API. In addition, a central processing unit that runs the SLAM algorithms (Holographic Processing Unit, HPU) limits its computational performance. The three AR systems have in common that they limit the tracking accuracy to provide a higher frame rate, a slower battery drain, and a lower hardware temperature as otherwise there may be a complete system failure (Linowes and Babilinski, 2017).

Applicability in Industry. Advantages and disadvantages of AR for industrial maintenance are already studied (Palmarini et al., 2017). They state that undamaged, clean, and undisguised markers (Kato and Billinghurst, 1999), e.g., QR and Vuforia codes, are needed to alleviate the problems.

To the best of our knowledge, there are no publicly available localization studies of AR systems in large-scale industry settings about (above $250m^2$). Dilek et al. (2018) describe both the functional limits of

AR_A and its limitations in real-time localization (dark scenes, few features, and excessive motion causing blurry images). They find that the localization system only works well in small areas of up to $1m^2$. Their findings indicate that current commercial AR systems are not yet applicable in industry settings.

Poth (2017) evaluates the AR systems for machine maintenance in the context of the Internet of Things (IoT). They rate systems according to their functionality and quality. Similar to Dilek et al. (Dilek and Erol, 2018) they find that AR systems only work well in small rooms and close to unique features in the environment. By attaching synthetic markers to the dynamic objects in the real environment they stabilize the AR systems and achieve a more accurate and reliable tracking over an area of $25m^2$. Our evaluation is partially motivated by their evaluation criteria.

AR Datasets. Dilek et al. (2018) and LI (Li et al., 2018; Handa et al., 2014) (human motion; in-/outdoor scenarios) provide complex camera movement specifically designed for AR systems. Unfortunately, both have restrictions: They do not provide an industry scenario and only provide inertial sensor information and camera images, but there are no Hololens-specific RGB-D images. Other available datasets like KITTI (Geiger et al., 2013) (car motion; outdoor scenario) and EuRoC (Burri et al., 2016; Löffler et al., 2018) (MAV motion; indoor scenario), and TUM (Schubert et al., 2018) and ADVIO (Cortés et al., 2018) (human motion; in-/outdoor scenarios) do not contain typical AR effects such as free and dynamic user movements that include abrupt changes in either direction or speed, loss of camera signals, etc. Moreover, these datasets cannot be used to re-evaluate AR_A , AR_G , and AR_M because these systems do not provide access to their processing pipeline: One cannot feed pre-recorded input data directly to the algorithms as these only work with the sensors (Linowes and Babilinski, 2017). Thus, there is no dataset available to investigate the reliability and accuracy of current AR systems in large-scale industry scenarios.

In total, since all the preliminary work does not help to decide if current commercial AR systems are applicable in industry settings, our paper creates a new industry-related dataset and evaluates the applicability of these AR systems.

3 PROBLEM DESCRIPTION

To set the terminology for the rest of the paper, let us sketch the key ideas of SLAM and its main localization problems in more detail. This allows us to set up error metrics in Sec. 4.

To seamlessly merge virtual objects or information into the real physical environment and to present the result in the user's HMD, AR systems require fast and accurate initialization, re-location after a temporary tracking loss, and accurate scaling of the virtual map for accurate and reliable localization. What makes this difficult is that AR users move completely free and dynamic which causes a variety of unexpected situations, such as abrupt changes in either direction or speed, that lead to occasional camera shake, loss of camera signal, rapid camera movement with strong motion blur, and dynamic interference.

SLAM methods address these problems. While SLAM methods differ in their feature-processing, mapping, and optimization, in general they all exploit loop closures, i.e., they use unique features in the environment with known positions to recalibrate the system and to correct mismatches of the mapping.

Obviously, lack of these features or their occlusion limits the effectiveness of this approach. The accuracy and reliability of SLAM depends on the correct feature detection and the correct detection of movement. First, there are both sensor noise and sensor measurement errors that lead to accumulating estimation errors of the movement when there are rapid changes in motion (Marchand et al., 2016; Taketomi et al., 2017). This even affects the best performing VISLAM approaches that combine inertial sensors and monocular camera images to more accurately estimate the user's movement. Second, there is the uncertainty of whether the AR system or the environment is moving or both. This also limits SLAM as it leads to inaccurate and unreliable pose estimates. Finally, small mistakes accumulate over time, decrease the localization accuracy, and cause unreliability.

Let us discuss the limits and the types of resulting errors in some more detail.

Dependency on Features. The tracking performance of SLAM depends on the environment. The more unique synthetic or natural features an environment offers, the higher are the accuracy and reliability when detecting and tracking features, but the computational effort and battery consumption also increase (Li et al., 2018). Most SLAM methods (Fraga-Lamas et al., 2018) use synthetic features (Marques et al., 2018), such as unique QR (Voinea et al., 2018) or Vuforia (Linowes and Babilinski, 2017) codes. But as synthetic features are elaborate to set up, today's systems try to locate natural features (Fraga-Lamas et al., 2018; Neumann and You, 1999; Simon et al., 2000). Regardless of the type of features used, if there are too few unique features the localization accumulates drift (scaling errors) or fails completely (Voinea et al., 2018). After a failure, the system relocates its

last position and aligns its map. This has two types of consequences: First, it is time consuming and leads to blind spots that cause map distortions in dynamic environments (Durrant-Whyte and Bailey, 2006). And second, an error in the relocation phase introduces a mismatch of the mapping (Linowes and Babilinski, 2017) which adds to the already accumulated drift.

Self- vs. Object-motion. A key assumption of SLAM is that features of the environment have known and static positions, so when the user moves (dynamic self-motion), objects shift their relative positions in the camera frame. As different positions in the environment in general result in different shifts in the frame, SLAM can use this to estimate the user’s trajectory. Even though occlusion of objects is an obvious issue here, SLAM works reasonably accurate and reliable in this case. This is no longer true, when objects move as well (dynamic object motion) (Saputra et al., 2018). Since then the map of the objects is no longer valid, SLAM’s estimate of the user position in general is wrong and unreliable, unless self- and object-motion can be separated (Taketomi et al., 2017). There is a middle ground: both the user or the objects can also be semi-static when resting phases with a fixed position alternate with short motion phases. Here, again both temporarily occluded features and the unreasonable origin of feature motion accumulate pose errors.

There are two widely used error descriptions in the literature: the scaling (localization) error and the mapping (initialization and relocalization) error.

Scaling Errors. The more features are occluded, the less reliable SLAM’s mapping between registered and measured features gets. The solution of the Perspective-n-Point (PnP) problem suffers from vanishing known features and becomes imprecise. A known countermeasure is to use environments with more distinct features, hoping that fewer of them get occluded when the camera moves. Another countermeasure are reset points. But using them in general accumulates a drift, i.e., a divergence of the mapping between real and virtual positions. This mismatch is called a scaling error.

Mapping Error. An unknown initial calibration (initialization error) of the registered and the measured maps leads to critical mapping problems, such as a wrong starting position in the map. Even with an accurate and reliable relative tracking the result is a complete misrepresentation of the real and estimated motion trajectories (Choset et al., 2005). Even if the initial calibration is correct, calibration inaccuracies in SLAM’s relocalization cause mapping errors.

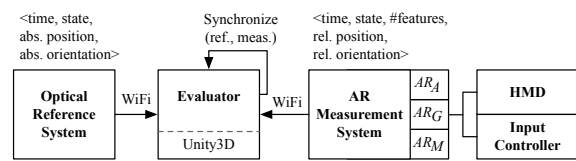


Figure 1: Evaluation framework.

4 DESIGN OF THE STUDY

This section describes our measurement setup, the study designs, and the metrics used to assess the tracking-, initialization-, and relocalization-accuracy, and the reliability of the AR systems.

4.1 Measurement Setup

We first sketch our evaluation framework and its hardware- and software-components. Then we describe both the small-scale measurement setup (to gauge the impact of feature motion on the accuracy and reliability of the AR platforms) and the large-scale measurement setup (to evaluate the performance of the AR platforms in real-world industry settings).

General Measurement Setup. The central evaluator of our evaluation framework in Fig. 1 has inputs from two sides: On the right there are the three hardware platforms AR_A , AR_G , and AR_M , see Fig. 2(a-c), to which we attached rigid markers (gray balls) that an optical reference system (on the left of Fig. 1) uses to measure the baselines of the user’s position and orientation. For the small- and the large-scale experiment there are different reference systems.

The former uses an Advanced Real-time Tracking (ART) system (12 ARTTRACK5 cameras with 4MP at 300Hz) with a mean absolute position error of $MAE_{ART}(pos.)=0.1mm$ (min: 0.001mm; max: 3.2mm; SD: 0.54mm) and an average absolute orientation accuracy of $MAE_{ART}(ori.)=0.01^\circ$ (min: 0.001°; max: 0.2°; SD: 0.06°) to estimate 6DoF poses on an area of $10m \times 10m \times 3m=300m^3$. The latter uses a Qualysis system (36 cameras (type designation: 7+) with 12MP at 300Hz) with a mean absolute posi-

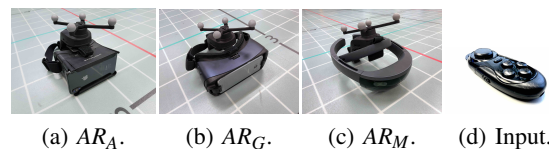


Figure 2: AR hardware components of our measurement platforms: (a) AR_A HMD: Starlight 2017; Rendering device: Apple iPhone X Late 2018 512GB, iOS 12.3; (b) AR_G HMD: Samsung GearVR 2018b; Rendering device: Samsung Galaxy S9 256GB, Android 9.1; (c) AR_M HMD: Hololens v1, v2017a; (d) Input controller: BLE 2018.

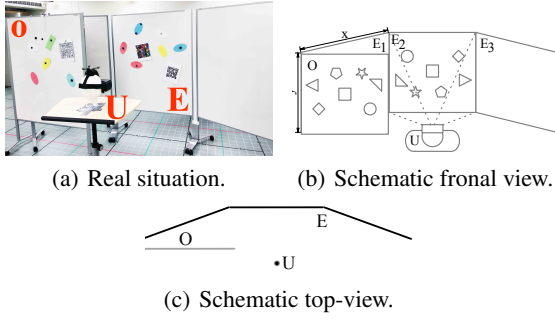


Figure 3: Small-scale setup: (U)ser, (E)nvirment, and (O)ccluder.

tion error of $MAE_{Qualysis}(pos.)=1.2mm$ (min: $0.1mm$; max: $8.9mm$; SD: $2.17mm$) and a mean absolute orientation error of $MAE_{Qualysis}(ori.)=0.52^\circ$ (min: 0.01° ; max: 1.7° ; SD: 0.76°) to estimate $6DoF$ poses on $45m \times 35m \times 7m=11.025m^3$.

The evaluator receives different data from the two sides. The reference system sends the current UTC timestamp and the absolute position and orientation at $300Hz$ on average (SD= $0.01Hz$). In addition, the ARs send their state (reliability level from 0% =not working to 100% =working) and the number of features (number of vertices of the current room mesh, i.e., the number of unique synthetic or natural features) that yield the *relative* position and orientation (AR_A : avg. $31Hz$, SD= $3.6Hz$; AR_G : avg. $27Hz$, SD= $7.9Hz$; AR_M : avg. $60Hz$, SD= $11.2Hz$). Note, that the coordinate systems of the ARs are always *relative* to the reference system’s coordinate system. To align both, we simply match the origins of the two coordinate systems and align the directions of the x- and y-axes.

The evaluator employs the cross-platform AR engine Unity3D (version 2018 LTS). To synchronize the data packets received from the two sides it uses both the UTC timestamp of the common WiFi access point and the frames per second rate (FPS). We also use Unity3D to implement the visualization of the user interface and to control the experiment, i.e., to start and stop the recording of the data which we trigger with a typical input device, see Fig. 2(d). For each experiment, the evaluator also provides visual feedback on the successful calibration and alignment of the reference and measurement setup.

The **small-scale setup** (Fig. 3) is a feature-rich environment consisting of 3 areas E_1 – E_3 (static boards of size $2m \times 2m$) that are positioned with an angle of 160° between them. While E_1 and E_3 are feature-free, the center board E_2 has a set of unique synthetic features whose poses the reference system can determine. There is also a moveable occluder board O that we roll into the user’s field of view (FoV) in certain scenarios of the experiment. Board O has the

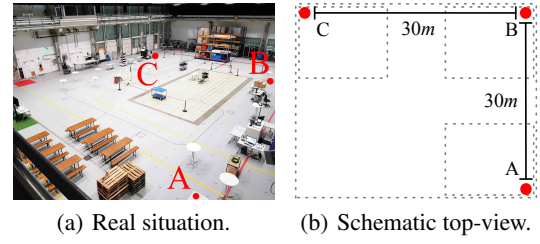


Figure 4: Large-scale setup: Cubicles A–C.

same size but a different set of synthetic features. According to Dilek et al. (2018) we chose boards with white backgrounds to avoid uncontrolled additional features. The distance between U , O , and E is chosen so that E and O completely fill the user’s FoV.

Large-scale Setup. Fig. 4 shows the large-scale setup that. On a floor of $30m \times 30m$ there are three cubicles A–C and several natural features.

4.2 Study Design

Table 1: Small-scale scenes.

	(U)ser	(O)ccluder
S_1	static	absent
S_2	dynamic	absent
S_3	static	dynamic
S_4	dynamic	dynamic
S_5	dynamic*	dynamic*

* synchronous movement of U and O , with the same start- and end-points.

Small-scale Study. We studied five different Small-scale motion scenarios S_1 – S_5 . In all of them the static environment E_1 – E_3 remained the same. As Table 1 shows, in S_1 and S_2 there was no occluder. In the other three scenarios O moved while the user either remained static or moved as well. In S_5 the movement of U and O was synchronous and the individual start- and end-points of both were the same. Fig. 5 shows snapshots of the scene over time. The red dashed arrows indicate the movement paths that will happen before the next snapshot is taken.

We claim that these scenarios mimic what frequently happens in industry settings when workers are busy in a cubicle and they or their surrounding objects may move within the cubicle.

Before we started recording the poses in each of the five scenarios, we calibrated the AR platforms. To do so, we aligned the relative coordinate system of the AR systems with the absolute coordinate system of the reference system on the basis of the first measured data points. This eliminates any differences in position and orientation. Based on this initial adjustment, both systems then track the same current pose within the experiment. After the calibration we

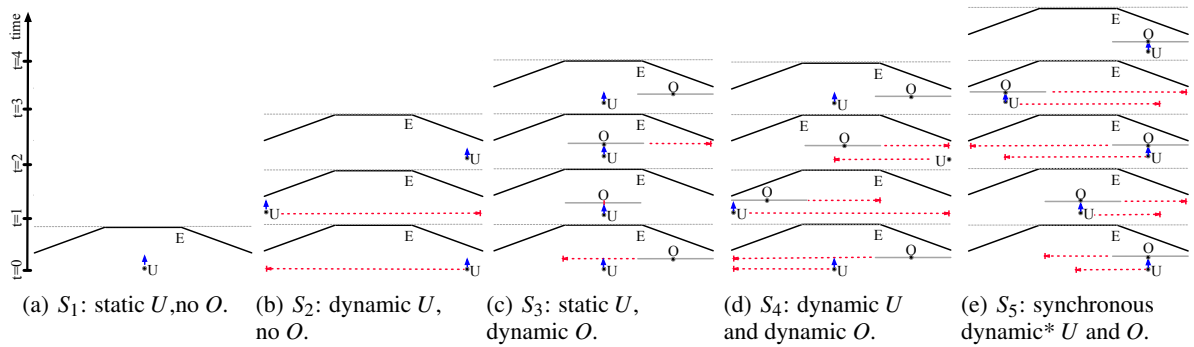


Figure 5: Small-scale experiment: Exemplary snapshots for the scenarios S_1 to S_5 ; (U)ser, (E)nvirment, and (O)cccluder; red arrows indicate motion over time from the bottom- to the top-row; blue arrows indicate the user’s viewing direction; gray dotted lines indicate a wall; duration between the three snapshots varies between the S_i ; *synchronous dynamic motion: both U and O have the same speeds and directions with the same individual start- and end-points.

slightly moved the AR platform to identify features of the central board E_2 and thus to initialize the tracking.

For each scenario, we recorded measurement data ten times and only present the mean values below.

S_1 (static U , no O) covers the real-world situation of a static user, standing still in a static environment. There is no occluder. In this and all of the subsequent small-scale scenarios the view of the user is always focused on E during the measurement.

In scenario S_2 (dynamic U , no O) the user performs a lateral movement from the right to the left side and back, at $0.5m/s$ on average, $SD=0.25m/s$.

S_3 (static U , dynamic O) is a real-world situation of a static user standing still in a dynamic environment. The occluder O moves into the user’s FoV from the right. Once it reaches the center it fully occludes the features of E_2 , presenting its own features to the user instead. O then changes its direction and moves back to the right. We used two different O -velocities: fast= $0.8m/s$, $SD=0.2m/s$ and slow= $0.3m/s$, $SD=0.1m/s$.

In S_4 (dynamic U and O) both the user and the occluder move, but independently of each other. The user performs a lateral movement from the center to the left, changes his/her direction, and moves to the right, changes his/her direction, and moves back to the center, at $0.5m/s$ on average, $SD=0.25m/s$. At the same time O moves from the right to the left, changes its direction, and moves back. On its way the occluder O temporarily hides the features of E_2 twice (and presents its own features instead). We used the same two O -velocities as in S_3 .

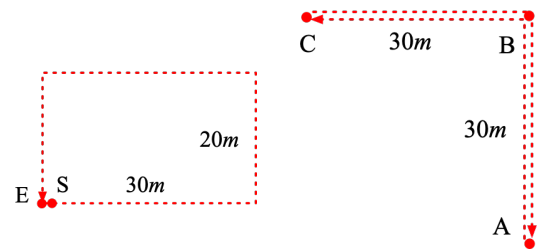
In S_5 (synchronous dynamic U and O) again both the user and the occluder move, but their speeds and directions are synchronized (velocity $SD(U, O)=0.9m/s$) so that the occluder O always hides the features of E_2 and presents its own features instead. Both the user and the occluder start

from the right, move to the center, change their directions, and move to the right, change their directions, and move to the left, and turn back to the right. S_5 uses the same O -velocities, but this time also for U .

Large-scale Study. We studied two different Large-scale scenarios L_1 and L_2 . Fig. 6 shows the movement paths of the user U . We claim that both scenarios are typical for an industry context with natural features: workers are likely to move between cubicles that are distant to each other. Again, we initially calibrated the AR platforms before we started to record the pose for each of the two scenarios. We again recorded measurement data ten times and only present the mean values below.

In L_1 a user moves within a static environment with natural features and follows a rectangular path of $2 \times 20m + 2 \times 30m = 100m$. The user starts in S and stops in E where we relocalize, i.e., recalibrate the system to determine the scaling and mapping errors.

In L_2 a user also moves within a static environment with natural features. The user starts in cubicle A , walks to B , and stops in C . Then, we relocalize and determine the scaling and mapping errors before the user walks back to A via B . The trajectory length is $4 \times 30m = 120m$. When back in A , we again relocalize



(a) L_1 : From (S)start to (E)nd. (b) L_2 : From cubicles A via B to C, and back.

Figure 6: Large-scale experiment: L_1 and L_2 show user trajectories (red dashed arrows); same cubicles as in Fig. 4.

and determine the errors.

To gauge how errors accumulate after the first 60m in cubicle C , there is a second set of measurements without the relocalization.

4.3 Metrics

Tracking Accuracy. We evaluate the accuracy by means of the mean absolute error (MAE) and the mean relative error (MRE). We measure both errors in terms of position error [m] and orientation error [$^\circ$]:

$$MAE = \frac{\sum_{i=1}^n |r_i - m_i|}{n}, \quad (1)$$

where r_i is the value from the reference system and m_i is the value measured in the AR system. The MAE uses the same scale as the data being measured. The mean relative error (MRE) is the following average:

$$MRE = \frac{\sum_{i=1}^n ||r_{i+1} - r_i| - |m_{i+1} - m_i||}{n}, \quad (2)$$

where r_{i+1} is the current and r_i is the previous reference. m_{i+1} is the current and m_i is the previous measure. The MRE also uses the same scale as the data being measured. The MRE expresses the scaling errors with multiple measures based on n samples, i.e., the difference between reference and measurement of n accumulated samples.

Initialization Accuracy. For each AR system we physically align the HMD's (measurement) coordinate system, i.e., the x-axis of the body frame, with the reference system's coordinate system, i.e., the x-axis of the system marked on the floor. Note, the evaluator provides feedback on the successful calibration, i.e., when the reference and measurement setup are aligned. We then calculate the translational and angular differences between the AR system and the reference system. We again measure initialization accuracy in terms of position error and orientation error.

Relocalization Accuracy. Similarly, we use the offset between the coordinate systems of the AR systems and the reference system to determine the relocalization accuracy (both position and orientation errors) after each of the scenarios S_1-S_5 and L_1-L_2 .

The **reliability** $R_{i,j} \in [-1; 1]$ of AR_j with $j \in A, G, M$ spans from system crash $[-1; 0]$ to fully functional $[0; 1]$ per frame i and is determined as:

$$R_{i,j} = \frac{feat(AR_j) - fail_{feat}(AR_j)}{max_{feat}(AR_j) - fail_{feat}(AR_j)}, \quad (3)$$

with the number of currently available features $feat(AR_j)$ in a scene, the number of features $fail_{feat}(AR_j)$ that cause AR_j to fail (AR_j requires at least $fail_{feat}(AR_j)+1$ to estimate a pose:

$AR_A=15$, $AR_G=26$, $AR_M=63$), and the maximal number $max_{feat}(AR_j)$ of features that we ever observed for AR_j being able to process in our experiments. It is an engineering task to find $fail_{feat}(AR_j)$. Note that $feat(AR_j) \leq fail_{feat}(AR_j)$ yields a system crash.

5 EVALUATION RESULTS

We present the measurements of the small- and the large-scale experiment, before we discuss the results.

5.1 Small-scale Measurements

Because of space restrictions we cannot show a figure per scenario, per occluder speed, and per AR system. We thus only show numbers and curves for the five scenarios S_1-S_5 (slow speed only) that were measured with AR_M , see Figs. 7(a-e). Table 2 holds condensed numbers for all cases. The general structure of the five Figs. 7(a-e) is as follows: They have three graphs each. The upper graph corresponds to the schematic top-view known from Fig. 5. The static environment and the occluder's starting, turning, and final positions (S_3-S_5) are shown in black. For the user trajectories the upper graph shows the AR_M measurements (red) and the reference values (blue). Deviations between the red and blue curves, i.e., absolute pose errors, are easy to spot. The occluder's trajectory is shown in grey. The second of the three graphs illustrates the motion velocities of the captured poses. The bottom graph shows the number of features $feat$ over time (black, dashed) and also the position errors MAE (green) and MRE (orange).

Measurement Results That Can Be Generalized across S_1-S_5 . As the user's focus was fixed to the environment in the small-scale experiment there were no significant orientation errors, see the orientation columns in Table 2. All the initialization errors are also unremarkable throughout S_1-S_5 and all ARs. The initialization errors are stable across S_1-S_5 as we always moved the features in about the same way when setting up. The relocalization errors show no significant changes across S_1-S_5 and vary around 5cm. But there is the trend that fast motion lowers and slow motion increases the relocalization errors.

The tracking accuracy is more interesting as the position errors, the number of features, and the reliability scores vary between the ARs and the scenarios. Across S_1-S_5 , AR_M shows the smallest errors, the highest number of features, and the best reliability. AR_A comes second. AR_G suffers from the largest errors, the lowest number of features, and the worst reliability. The standard deviations (SD) support this:

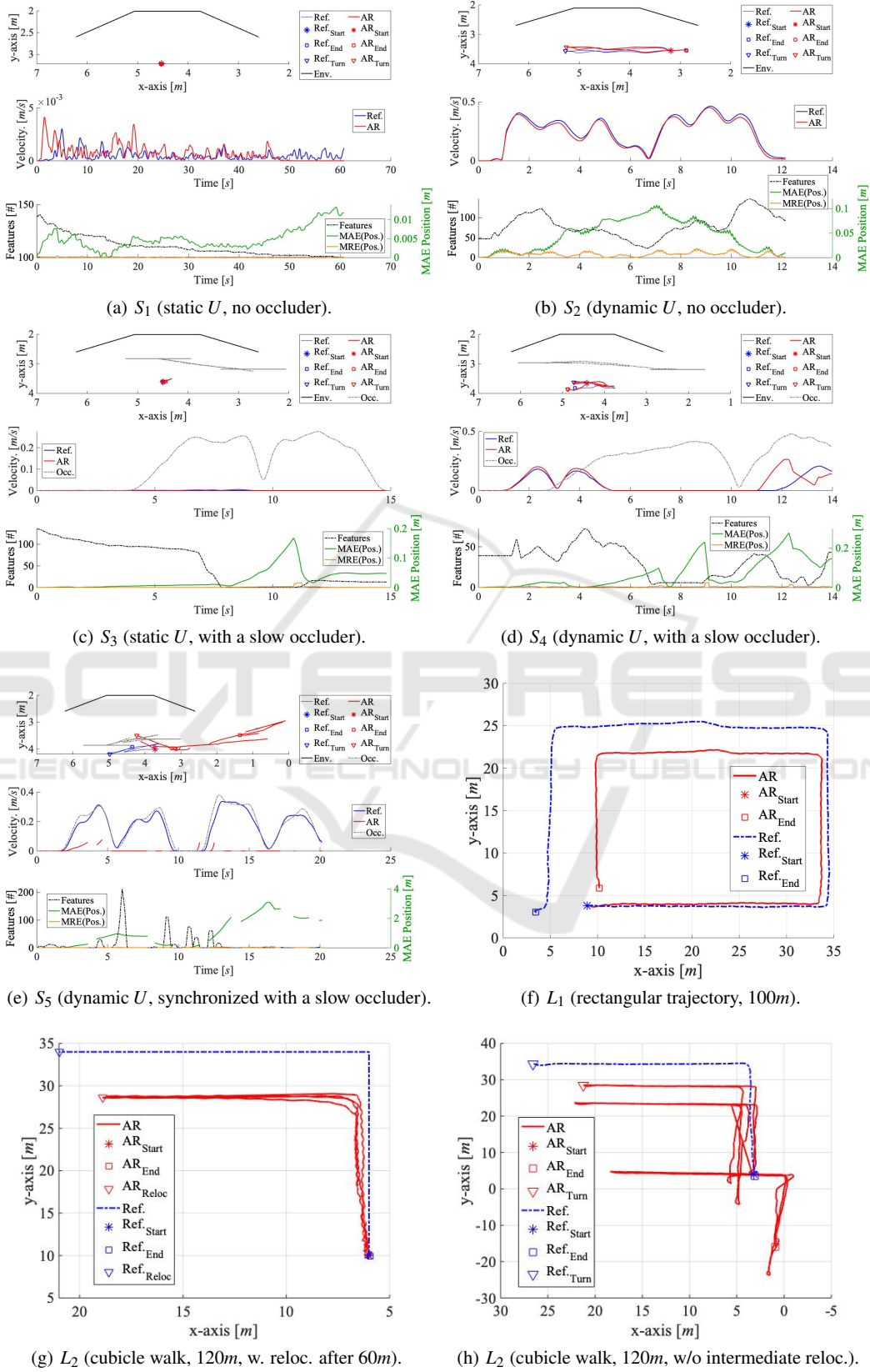


Figure 7: AR_M measurements; (a-e) for S_1 – S_5 : trajectories, velocities, features, and accuracy; (f-h) for L_1 – L_2 : trajectories.

Table 2: Condensed measurements (best ones in bold).

Scenario	MAE (ARs) [cm]		Tracking						Initialization			Relocalization			Features *			Reliability *			
	MAE(AR _A)	MAE(AR _G)	Position			Orientation			MAE(AR _A)	MAE(AR _G)	MAE(AR _M)	MAE(AR _A)	MAE(AR _G)	MAE(AR _M)	AR _A [#]	AR _G [#]	AR _M [#]	AR _A [%]	AR _G [%]	AR _M [%]	
S_1 (static U , no O)	2.5	5.7	2.2	0.4	0.9	0.8	1.7	3.2	1.5	16.2	29.4	11.6	6.2	9.4	7.6	14	123	359	0	36	59
SD	2.1	2.7	1.2	0.02	0.07	0.01	0.8	2.3	0.6	7.3	11.9	5.6	2.3	4.9	1.6	1	13	57	0	0	0
S_2 (dyn. U , no O)	8.1	12.3	7.4	2.1	3.7	0.7	2.3	1.5	0.9	16.2	21.3	9.8	5.9	7.1	4.7	46	183	391	24	58	65
SD	2.2	2.8	1.9	0.9	1.3	0.8	4.4	4.7	1.7	5.4	17.1	4.9	1.7	5.3	3.2	61	137	298	35	41	43
$S_{3,slow}$ (static U , dyn. O)	17.2	19.3	13.1	4.9	5.2	4.6	2.4	4.5	2.1	18.1	29.3	8.9	9.3	19.7	6.8	18	46	143	3	7	16
SD	2.5	3.8	2.5	1.6	1.7	1.3	3.5	4.5	2.9	4.5	11.4	3.8	2.1	4.9	4.1	53	87	125	29	23	12
$S_{3,fast}$ (static U , dyn. O)	16.3	17.1	11.0	3.9	4.1	3.4	2.4	4.5	2.1	17.9	28.1	8.7	8.2	17.3	5.5	24	61	213	7	13	30
SD	2.4	3.6	1.9	1.9	2.1	1.8	4.4	4.7	2.8	5.4	10.1	4.1	1.9	4.1	1.3	45	77	121	23	19	12
$S_{4,slow}$ (dyn. U & O)	18.1	21.2	17.8	2.4	3.5	0.9	3.7	3.9	2.5	17.2	18.3	16.8	7.9	6.8	5.2	37	103	331	17	29	53
SD	4.1	4.5	3.3	1.5	2.7	1.3	3.4	5.1	2.4	9.1	9.4	5.8	2.1	3.8	5.2	68	188	206	41	60	28
$S_{4,fast}$ (dyn. U & O)	16.2	19.5	14.1	1.6	2.7	0.8	4.9	5.8	3.1	16.8	17.3	15.7	6.7	8.8	4.3	73	208	421	44	67	71
SD	4.1	4.5	3.3	1.5	2.7	1.3	3.4	5.1	2.4	5.8	9.4	9.1	2.1	3.8	5.2	57	166	187	46	65	25
$S_{5,slow}$ (sync. dyn. U & O)	87.3	112.9	76.3	21.8	26.4	19.1	3.9	4.3	2.4	15.7	16.8	14.9	7.3	9.8	6.4	21	37	88	5	4	5
SD	69.3	82.1	50.6	11.9	14.3	7.7	3.4	4.1	3.7	5.2	4.7	8.2	1.3	2.6	1.1	88	247	366	56	82	60
$S_{5,fast}$ (sync. dyn. U & O)	85.1	108.3	73.2	19.7	23.8	17.3	4.6	6.1	4.0	14.9	15.9	12.8	6.5	10.7	5.9	27	54	117	10	11	11
SD	61.4	78.3	47.4	13.7	16.3	6.6	3.1	5.7	2.9	5.3	6.4	4.9	3.5	4.3	1.2	76	201	315	46	65	50
L_1 (static U , no O)	-	-	601.2	-	-	0.7	-	-	3.5	-	-	32.8	-	-	41.5	-	-	487	-	-	84
SD	-	-	24.3	-	-	2.3	-	-	1.6	-	-	5.7	-	-	4.3	-	-	42	-	-	0
L_2 (static U , no O)	-	-	437.9	-	-	0.9	-	-	4.1	-	-	29.9	-	-	36.2	-	-	477	-	-	82
SD	-	-	33.9	-	-	1.9	-	-	4.2	-	-	6.3	-	-	5.7	-	-	56	-	-	0
$L_{2,w/o}$ relocalization	-	-	1728.5	-	-	0.6	-	-	3.8	-	-	28.3	-	-	-	-	-	491	-	-	85
SD	-	-	43.6	-	-	4.1	-	-	1.2	-	-	5.7	-	-	-	-	-	66	-	-	0

* Feature counts (\min ., \max .) for all scenarios: $feat(AR_A) \in [14; 147]$, $feat(AR_G) \in [25; 296]$, and $feat(AR_M) \in [62; 567]$.

there is lower variance for AR_M (within and across all measures) than for AR_A . AR_G has the highest SD.

Now that we have sketched the big picture, let us discuss the scenarios individually.

Measurement Results That Are Specific for S_1 – S_5 . S_1 and S_2 yield the lowest absolute and relative position errors and orientation errors in all measures for all ARs. While S_1 yields the lowest MAE of the position (2.2cm) and orientation (0.9°), S_2 provides the lowest MRE of the position (0.3cm) across all experiments. In Figs. 7(a+b) we observe that when there is no velocity in S_1 the number of features remains stable. With dynamics in S_2 there is also a varying number of features. The reliability scores in Table 2 support these findings as there are higher scores when the user moves faster (or moves at all).

Compared to S_1 – S_2 , there are higher absolute and relative position errors and orientation errors in S_3 and S_4 , see Table 2. As before, a moving user yields higher absolute position errors (MAE > 10cm) but lower relative errors (MRE < 1cm), even if there is an occluder. This also holds for the two fast motion variants. Figs. 7(c+d) again show that a more dynamic user sees more features, which then results in a higher reliability score. In S_3 the movement of the occluder has a dramatic impact on the number of features and the reliability scores: both drop to lower values once the occluder hides E_2 , and they remain on that level when the occluder leaves the user’s FoV

again. We discuss this in detail in Sec. 6.

S_5 yields the highest position and orientation errors of all measurements with all ARs. This time the absolute position error is more than 5 times higher for all ARs. Also the number of features and the reliabilities are the lowest among all experiments. The user moves synchronously at the same speed in the same direction as the occluder. For the user, the occluder’s features do not move, as they move quasi parallel to his/her FoV, see the red curve in the velocity graph of Fig. 7(e). Hence, the ARs cannot distinguish between their self-motion and the motion of the occluder’s features. In total, the ARs interpret this as if there is no movement at all. Because even in these situations, they apparently do not use inertial sensors to sense motion and continue to rely solely on the camera’s motion estimates. However, due to the study design there may be moments when the ARs still occasionally find features to stabilize their internal feature tracking state.

5.2 Large-scale Measurements

For our large-scale experiments we can only show the measurements of AR_M because both AR_A and AR_G were unable to initialize and localize. The bottom rows of Table 2 and Figs. 7(f-h) hold the data. The graph layouts correspond to the schematic top-view known from Fig. 6. For the user trajectories they show

Table 3: Average scaling error in the large-scale scenarios.

	Distance, SD, td [m]			Scaling Error, SD
L_1	100,	9,	101.2	5.94cm/m, 0.21cm
L_2	60,	3,	62.8	6.97cm/m, 0.19cm
$L_{2,w/o}$	120,	12,	118.76	14.55cm/m, 2.83cm

both the AR measurements (red) and the reference values (blue). Again, deviations, i.e., absolute pose errors, are easy to spot.

Measurement Results That Can Be Generalized across L_1 – L_2 . As before, the orientation, initialization, and relocalization errors are unremarkable, see Table 2. However, because of the much larger distances both the initialization and relocalization errors are higher than for S_1 – S_5 , but they show similar variances. The number of features is higher for L_1 – L_2 (at lower variance) than for S_1 – S_5 and results in the highest reliability values across all experiments.

Table 2 shows that the absolute position errors grow with the length of the trajectory that is traveled without relocalization (60m in L_2 , 100m in L_1 , and 120m in L_2). This can also be seen in Figs. 7(f-h). When you follow the trajectory of the user along the space, the distances between the red and blue curves grow. When there is no intermediate relocalization, the effect is much stronger than in plain L_2 . After each measurement or in the intermediate relocalization phase we calculated the scaling error $S = \frac{MAE_{position}}{td}$ where td is the traveled distance, see Table 3. Note, that the distance and td differ because of the SD.

Whereas the scaling error is about the same for L_1 and L_2 with a relocalization after 60m, (6.65cm/m (=5.94+6.97/2) on average), it "explodes" (14.4cm/m) in L_2 when no relocalization is done for about 120m. We discuss this in detail below.

6 DISCUSSION

The occluder-free scenarios S_1 and S_2 yield the lowest absolute position error for all AR s. This is because the SLAM techniques are able to separate a user's self-motion from the static environment. In contrast, the techniques struggle to accurately tell self-motion and feature motion (of the occluder) apart. This is supported by the scenarios S_3 – S_5 that yield higher absolute errors when an occluder is present and when the occluder hides the features of the environment longer or more often.

Velocity has an impact. Although, a higher velocity leads to blurry camera images and hence fewer features, our motion scenarios resulted in more features and a better relative position accuracy. We think that faster movement reduces the duration of situa-

tions where there is an occluder in the FoV of the user, and therefore the duration of a disturbance is shorter, which leads to smaller accumulated errors.

We suppose that SLAM implementations make use of an internal filter that estimates the position in case of a noisy input (a varying number of features or unknown features), i.e., when there are dynamics of either U or O or both. After a while, the AR systems stabilize the filter with ground truth knowledge (known features) and relocalize. What supports this assumption is the slight delay and offset that exist between the number of features and the position errors in the graphs in Figs. 7(d) (compare the "Features" and the "MAE" curves within the [4.5s; 6s] interval in the bottom graph).

In all our scenarios there is an inverse correlation between a high reliability score (number of features) and a low MRE of the position (and vice versa). There is no such inverse correlation with the MAE. On the contrary, especially in the L_i scenarios when the R is high, the MRE is low, but the MAE is also high. We suppose that the initialization and relocalization errors have a stronger impact on the MAE than the number of features. This is in line with findings by (Marchand et al., 2016; Terashima and Hasegawa, 2017) as VISLAM for the AR s works like a pedestrian dead reckoning (PDR) algorithm. Here, the initialization and relocalization errors stabilize the absolute position while the relative position updates (estimated based on the features) accumulate small errors (with more features) over time (scaling error).

The impact of the scaling errors (accumulation of small relative position errors) depends on the scale. There is little impact in the small-scale scenarios, but the AR measurements and the reference positions differ a lot in the large-scale scenarios. This indicates that the AR systems exploit both the initialization and relocalization to stabilize the absolute positions. However, when they internally are confident about the input (no varying or unknown features) they rely on the relative position estimates. Hence, for SLAM to perform best, both MAE and MRE must be reduced.

We think that the reason for AR_M performing significantly better (in all measures, in all scenarios) than AR_A or AR_G is that AR_M exploits a special $RGB - D$ sensors, while the other only use a single RGB sensor. As there is no such hardware difference between AR_A and AR_G a potential explanation why AR_A outperforms AR_G may be that its SLAM is better optimized for its sensors.

In scenarios with relocalization and high reliability the AR s achieve a low MRE but a high MAE of the position. But with a long trajectory even a small relative error accumulates and grows into a significant

relative drift and absolute offset. In the large-scale scenarios the absolute error linearly increases as there is an average scaling error of approximately $5.9\text{cm}/\text{m}$ if there are intermediate relocalizations after at most 100m . However, we postulate that this linearity only holds when there are no changes or only slight rotations of up to 90° in the movement direction. The counterexample ($S=14.5\text{cm}/\text{m}$) is L_2 without relocalization and with its abrupt 180° rotation.

The general applicability of the reliability score R (solely based on features) cannot be guaranteed, as we saw that there are situations when a higher R does not correlate with the MAE but with the MRE of the position. Because a single metric as the MRE, is not enough to evaluate and validate accuracy and reliability of ARs our R could be improved.

Although there are many other AR platforms today, e.g., Wikitude (Fraga-Lamas et al., 2018), we chose AR_A , AR_G , and AR_M because they are marketable, inexpensive, pre-installed, and widely used by our industrial customers. We focused on these three commercial systems as these are well established in both the consumer and industrial markets and therefore their manufacturers offer customer support. Industrial customers are unwilling to work with research and development versions of AR systems just because they provide more accurate positions in some special cases.

7 CONCLUSION

We studied the applicability of today's popular AR systems (Apple ARKit, Google ARCore, and Microsoft Hololens) in industrial contexts (large area of $1,600\text{m}^2$, walking distances of up to 120m between cubicles, and dynamic environments with volatile natural features). The Hololens with its special RGB-D sensors outperformed ARKit (RGB only) in all experiments. ARCore showed the worst results.

In a nutshell, we found that standing still does not result in any features while motion enables the detection of features. However, abrupt movement changes at high speeds reduce the number of detectable features. A low/high number of features yields a low/high reliability. And a low/high reliability results in high/low relative and absolute position errors. Low/high position errors enable/disable AR systems in large scale industry environments.

Regardless of the AR systems, we only found good position accuracies in static environments and when only the user moves. Having more identifiable features helps. Whereas movement results in detectable features and hence in reliabilities and relative position

accuracies, on longer trajectories and at higher velocities there is still a significant amount of accumulated drift. Hence, AR systems are applicable in industry settings when a worker's surroundings are static and when process streets between cubicles are short and only require smooth directional changes.

When relocalization is possible within at least 100m of the trajectory, the AR systems accumulate a linear scaling error of $6.65\text{cm}/\text{m}$, on average. When there is no intermediate relocalization available, the best system only yields a MAE of 17.28m per 120m , with a scaling error of up to $14.4\text{cm}/\text{m}$, which is clearly too much for industry-strength applications.

We identified two typical industry scenarios that revealed problems of the AR systems: (a) They tend to crash when a user moves while a surrounding object, e.g., a fork lift, synchronously moves on the side. (b) There are system instabilities when workers randomly enter or leave the field of view of the AR system and temporarily occlude known features (as the systems can hardly distinguish between self-motion and feature motion).

ACKNOWLEDGMENTS

This work was supported by the Bavarian Ministry for Economic Affairs, Infrastructure, Transport and Technology through the Center for Analytics—Data—Applications (ADA-Center) within the framework of "BAYERN DIGITAL II".

REFERENCES

- Burri, M., Nikolic, J., Gohl, P., Schneider, T., Rehder, J., Omari, S., Achtelik, M. W., and Siegwart, R. (2016). The EuRoC micro aerial vehicle datasets. *Intl. J. of Robotics Research*, 35(10):1157–1163.
- Choset, H. M., Hutchinson, S., Lynch, K. M., Kantor, G., Burgard, W., Kavraki, L. E., and Thrun, S. (2005). *Principles of robot motion: theory, algorithms, and implementation*. Intelligent Robotics and Autonomous Agents. MIT Press, Cambridge, USA.
- Cortés, S., Solin, A., Rahtu, E., and Kannala, J. (2018). AD-VIO: An authentic dataset for visual-inertial odometry. In *Proc. European Conf. Computer Vision (ECCV)*, pages 419–434, Munich, Germany.
- Dilek, U. and Erol, M. (2018). Detecting position using ARKit II: generating position-time graphs in real-time and further information on limitations of ARKit. *Physics Education*, 53(3):5–20.
- Durrant-Whyte, H. and Bailey, T. (2006). Simultaneous localization and mapping: part I. *Robotics & Automation Magazine*, 13(2):99–110.

- Feigl, T., Mutschler, C., and Philippsen, M. (2018). Supervised learning for yaw orientation estimation. In *Proc. Intl. Conf. Indoor Navigation and Positioning (IPIN)*, pages 103–113, Nantes, France.
- Fraga-Lamas, P., Fernández-Caramés, T. M., Blanco-Novoa, Ó., and Vilar-Montesinos, M. A. (2018). A review on industrial augmented reality systems for the industry 4.0 shipyard. In *Proc. Intl. Conf. Intelligent Robots and Systems (IROS)*, pages 131–139, Madrid, Spain.
- Geiger, A., Lenz, P., Stiller, C., and Urtasun, R. (2013). Vision meets robotics: The KITTI dataset. *Intl. J. of Robotics Research*, 18(17):6908–6926.
- Handa, A., Whelan, T., McDonald, J., and Davison, A. J. (2014). A benchmark for RGB-D visual odometry, 3D reconstruction and SLAM. In *Proc. Intl. Conf. Robotics and Automation (ICRA)*, pages 1524–1531, Hong Kong, China.
- Kasyanov, A., Engelmann, F., Stückler, J., and Leibe, B. (2017). Keyframe-based visual-inertial online SLAM with relocalization. In *Proc. Intl. Conf. Intelligent Robots and Systems (IROS)*, pages 6662–6669, Vancouver, Canada.
- Kato, H. and Billinghurst, M. (1999). Marker tracking and HMD calibration for a video-based augmented reality conferencing system. In *Proc. Intl. Workshop on Augmented Reality (IWAR)*, pages 85–94, San Francisco, CA.
- Kerl, C., Sturm, J., and Cremers, D. (2013). Dense visual SLAM for RGB-D cameras. In *Proc. Intl. Conf. Intelligent Robots and Systems (IROS)*, pages 2100–2106, Tokyo, Japan.
- Klein, G. and Murray, D. (2007). Parallel tracking and mapping for small AR workspaces. In *Proc. Intl. Workshop on Augmented Reality (ISMAR)*, pages 1–10, Nara, Japan.
- Löffler, C., Riechel, S., Fischer, J., and Mutschler, C. (2018). Evaluation criteria for inside-out indoor positioning systems based on machine learning. In *Proc. Intl. Conf. Indoor Positioning and Indoor Navigation (IPIN)*, pages 1–8, Nantes, France.
- Li, P., Qin, T., Hu, B., Zhu, F., and Shen, S. (2017). Monocular visual-inertial state estimation for mobile augmented reality. In *Proc. Intl. Conf. Intelligent Robots and Systems (IROS)*, pages 11–21, Vancouver, Canada.
- Li, W., Saeedi, S., McCormac, J., Clark, R., Tzoumanikas, D., Ye, Q., Huang, Y., Tang, R., and Leutenegger, S. (2018). InteriorNet: Mega-scale multi-sensor photo-realistic indoor scenes dataset. *arXiv preprint arXiv:1809.00716*, 18(17).
- Linowes, J. and Babilinski, K. (2017). *Augmented Reality for Developers: Build practical augmented reality applications with Unity, ARCore, ARKit, and Vuforia*. Packt Publishing Ltd, Birmingham, UK.
- Liu, H., Chen, M., Zhang, G., Bao, H., and Bao, Y. (2018). Ice-ba: Incremental, consistent and efficient bundle adjustment for visual-inertial SLAM. In *Proc. Intl. Conf. Computer Vision and Pattern Recognition (CVPR)*, pages 1974–1982, Salt Lake City, UT.
- Marchand, E., Uchiyama, H., and Spindler, F. (2016). Pose estimation for augmented reality: A hands-on survey. *Trans. Visualization and Computer Graphics*, 22(12):2633–2651.
- Marques, B., Carvalho, R., Dias, P., Oliveira, M., Ferreira, C., and Santos, B. S. (2018). Evaluating and enhancing Google Tango localization in indoor environments using fiducial markers. In *Proc. Intl. Conf. Autonomous Robot Systems and Competitions (ICARSC)*, pages 142–147, Torres Vedras, Portugal.
- Mur-Artal, R. and Tardos, J. D. (2017). ORB-SLAM2: An open-source SLAM system for monocular, stereo, and RGB-D cameras. *Trans. Robotics*, 33(5):1255–1262.
- Neumann, U. and You, S. (1999). Natural feature tracking for augmented reality. *Trans. on Multimedia*, 1(1):12–20.
- Palmarini, R., Erkoyuncu, J. A., and Roy, R. (2017). An innovative process to select augmented reality (AR) technology for maintenance. In *Proc. Intl. Conf. Manufacturing Systems (CIRP)*, pages 23–28, Taichung, Taiwan.
- Regenbrecht, H., Meng, K., Reepen, A., Beck, S., and Langlotz, T. (2017). Mixed voxel reality: Presence and embodiment in low fidelity, visually coherent, mixed reality environments. In *Proc. Intl. Conf. Intelligent Robots and Systems (IROS)*, pages 90–99, Vancouver, Canada.
- Saputra, M. R. U., Markham, A., and Trigoni, N. (2018). Visual SLAM and structure from motion in dynamic environments: A survey. *Comput. Surv.*, 51(2):1–36.
- Schubert, D., Goll, T., Demmel, N., Usenko, V., Stöckler, J., and Cremers, D. (2018). The TUM VI benchmark for evaluating visual-inertial odometry. In *Proc. Intl. Conf. Intelligent Robots and Systems (IROS)*, pages 6908–6926, Madrid, Spain.
- Simon, G., Fitzgibbon, A., and Zisserman, A. (2000). Markerless tracking using planar structures in the scene. In *Proc. Intl. Workshop Augmented Reality (ISMAR)*, pages 120–128, Munich, Germany.
- Taketomi, T., Uchiyama, H., and Ikeda, S. (2017). Visual SLAM algorithms: a survey from 2010 to 2016. *Trans. Computer Vision and Applications*, 9(1):452–461.
- Terashima, T. and Hasegawa, O. (2017). A visual-SLAM for first person vision and mobile robots. In *Proc. Intl. Conf. Intelligent Robots and Systems (IROS)*, pages 73–76, Vancouver, Canada.
- Vassallo, R., Rankin, A., Chen, E. C. S., and Peters, T. M. (2017). Hologram stability evaluation for Microsoft HoloLens. In *Proc. Intl. Conf. Robotics and Automation (ICRA)*, pages 3–14, Marina Bay Sands, Singapore.
- Voinea, G.-D., Girbacia, F., Postelnicu, C. C., and Marto, A. (2018). Exploring cultural heritage using augmented reality through Google’s Project Tango and ARCore. In *Proc. Intl. Conf. VR Techn. in Cultural Heritage*, pages 93–106, Brasov, Romania.
- Yan, D. and Hu, H. (2017). Application of augmented reality and robotic technology in broadcasting: A survey. *Intl. J. on Robotics*, 6(3):18–27.